## 4.4 LiDAR Digital Surface Models

Analysis of LiDAR elevation products has focused on examining the effectiveness of LiDAR elevation products for identifying significant topographical features of the terrace and floodplain, quantifying relative accuracy and absolute accuracy of LiDAR elevation products compared to elevation values recorded by field survey using dGPS, and analysis of the impact of varying resolutions of LiDAR elevation data on the DSM metrics and the ability to identify significant landscape detail.

### *4.4.1 LiDAR Digital Surface Models and Geoarchaeological Mapping*

Data for this project were acquired by Infoterra using an Airborne Laser Terrain Mapper (ALTM) the Optech ALTM 2033 LiDAR, collecting 1 point/$m^2$ (Optech 2003). The survey light was carried out as a single sortie in February 2003. The Infoterra survey provides access to point-cloud data (Fig. 4.10) as well as grid arrays of FP and LP and laser intensity data (Figs. 4.11-4.13). Initial processing of the point-cloud data was undertaken by Steve Wilkes; point cloud data were used to generate DSM by surfacing in ERDAS Imagine using a rubber sheeting algorithm to produce a regular grid.

The raw LiDAR data were processed to WGS84 projection, with ellipsoidal elevation values, transformed to British National Grid with orthographic elevation values conforming to Ordnance Datum, and a regular grid with elevation values at grid nodes, generated from the point-could. Analysis of the LiDAR data was undertaken in ArcGIS 9 after importing and conversion to ArcGIS Grid format. Basic analysis comprised a visual comparison of LiDAR FP, LP and intensity data with air-photographic and other evidence.

### *4.4.2 L iDAR DSM results*

The utility of LiDAR elevation data for mapping floodplain and terrace geoarchaeology is immediately and spectacularly evident across the study area. The general disposition of the terrace units and the principal palaeochannels identified from air-photographs are clearly visible on the FP DSM (Fig. 4.11). However, some channels are partially obscured by vegetation, in particular the dense belt of scrubby woodland towards the northeastern edge of the study area. In contrast, the LP DSM (Fig. 4.12), from which laser returns from vegetation are excluded, clearly displays the detail of all palaeochannels without the obscuring effects of vegetation cover. This is most clearly demonstrated in a profile view through the FP and LP LiDAR data or this palaeochannels (Fig. 4.13). The ability of LiDAR to penetrate vegetation has proven particularly useful in this context.

LiDAR intensity data (Fig. 4.14) also records some palaeochannels as variations in the intensity of the reflected laser pulse. In general palaeochannels are indicated by a low level of reflections of the laser pulse; this is further discussed later. Closer comparison of extracts from the LP DSM and intensity values with aerial photographic evidence reveals the extent to which LiDAR is able to reveal geomorphological features not captured by conventional photography and also some limitations of LiDAR.

Figure 4.15 shows the modern floodplain close to the River Trent in the northeast corner of the study area. Palaeochannels and other floodplain features evident as water filled depressions in the aerial photography are clearly delineated by the LiDAR LP DSM. In addition, a number of other subtle

features, including curvilinear ridges, possibly ridge and swale, are evident on the LiDAR image, but not the aerial photograph. The LiDAR intensity data provides a further view of this area of floodplain. In general, areas of low laser reflection (darker on the image) coincide with the water filled depressions on the air photograph (although these features were not water filled at the time of the LiDAR flight as there is no evidence of characteristic reflections from water). Comparison of intensity data and air photographic evidence suggest that these depressions, with moist fills (confirmed by field inspection) are responsible for low levels of laser reflection. Not all of the topographical features evident on the DSM are seen as low intensity features on the intensity data, perhaps indicating that some depressions, although topographically clearly defined, do not have fills significantly wetter that the surrounding floodplain.

Figure 4.16 shows a part of the Hemington terrace close to the centre of the study area. Air photographic, LP DSM and intensity data all reveal a similar pattern of ridge and swale topography in the southern part of the area. The well-defined palaeochannels to the north of this are also clearly evident in both the FP DSM and intensity data, although less clear in the air photograph. However, the air-photographic evidence reveals a number of other channels as cropmarks, crossing this terrace unit that are not evident in the LiDAR data, as well as a cropmark sub-rectangular D shaped enclosure. Interestingly a roughly northwest to southeast aligned linear ridge, indicating the slight earthwork traces of a former medieval plough headland, are well defined by the LP DSM, but are not evident in the intensity data or on the air photograph. Clearly there is no simple relationship between what type of feature and in what circumstances features are revealed by LiDAR. Close comparison of the complimentary evidence of LiDAR with air photography seems necessary to generate a full picture of the geoarchaeology of the study area.

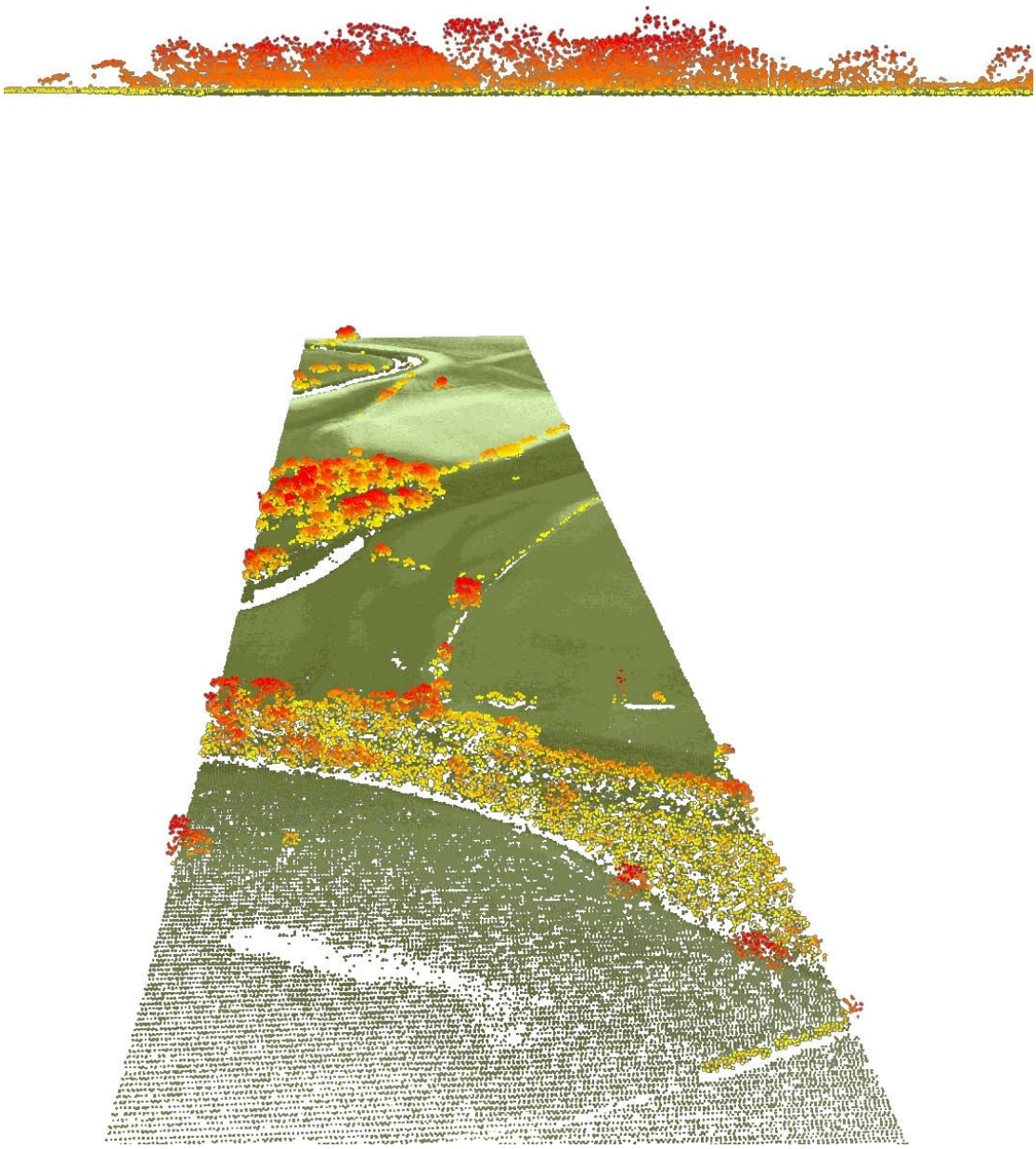

**Fig 4.10:** Two views of point cloud LiDAR elevation data for a part of the study area. Top a cross section through the point could and bottom an oblique view of the point cloud, both showing first pulse points (primarily vegetation) coloured red/orange and last pulse points (ground surface) coloured green.

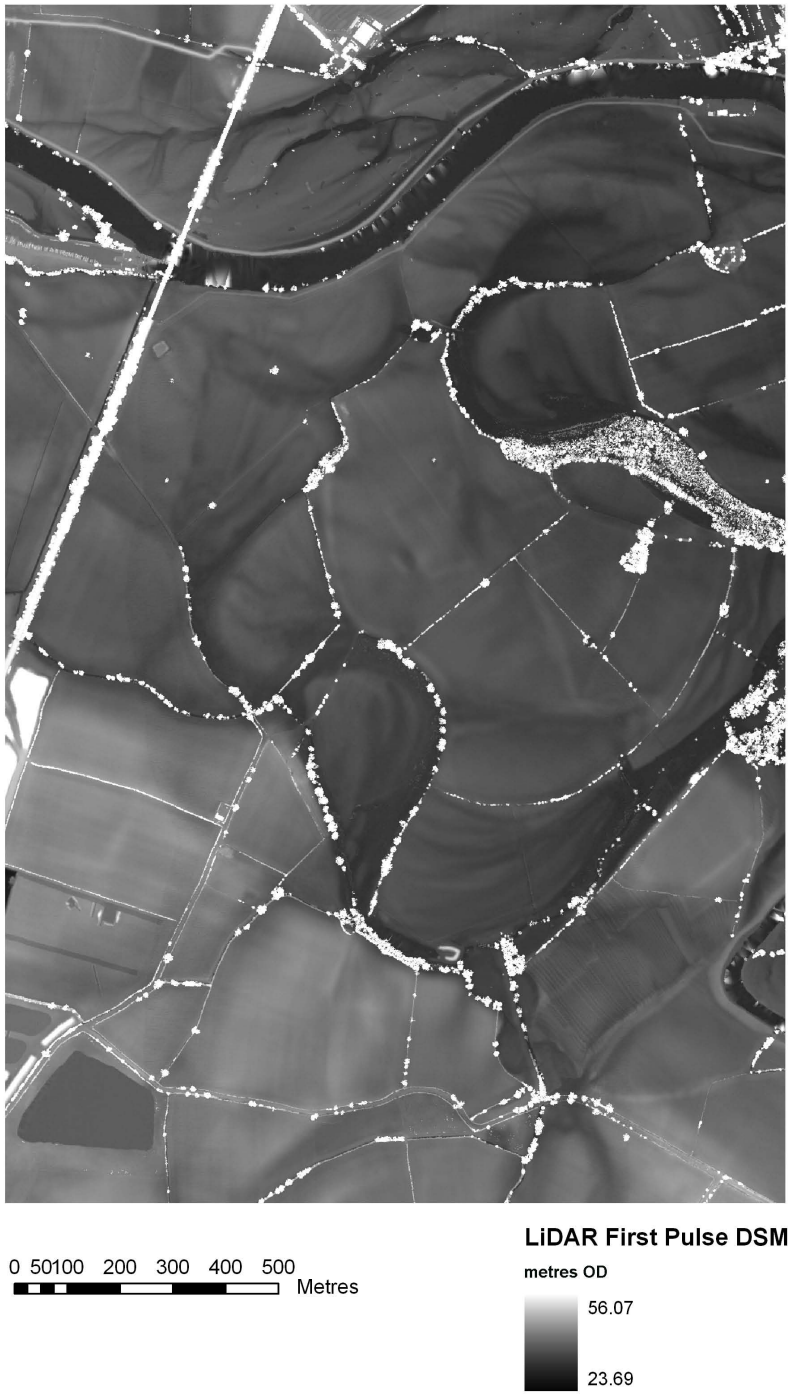


**Fig 4.11:** LiDAR fist pulse digital surface model of the study area.

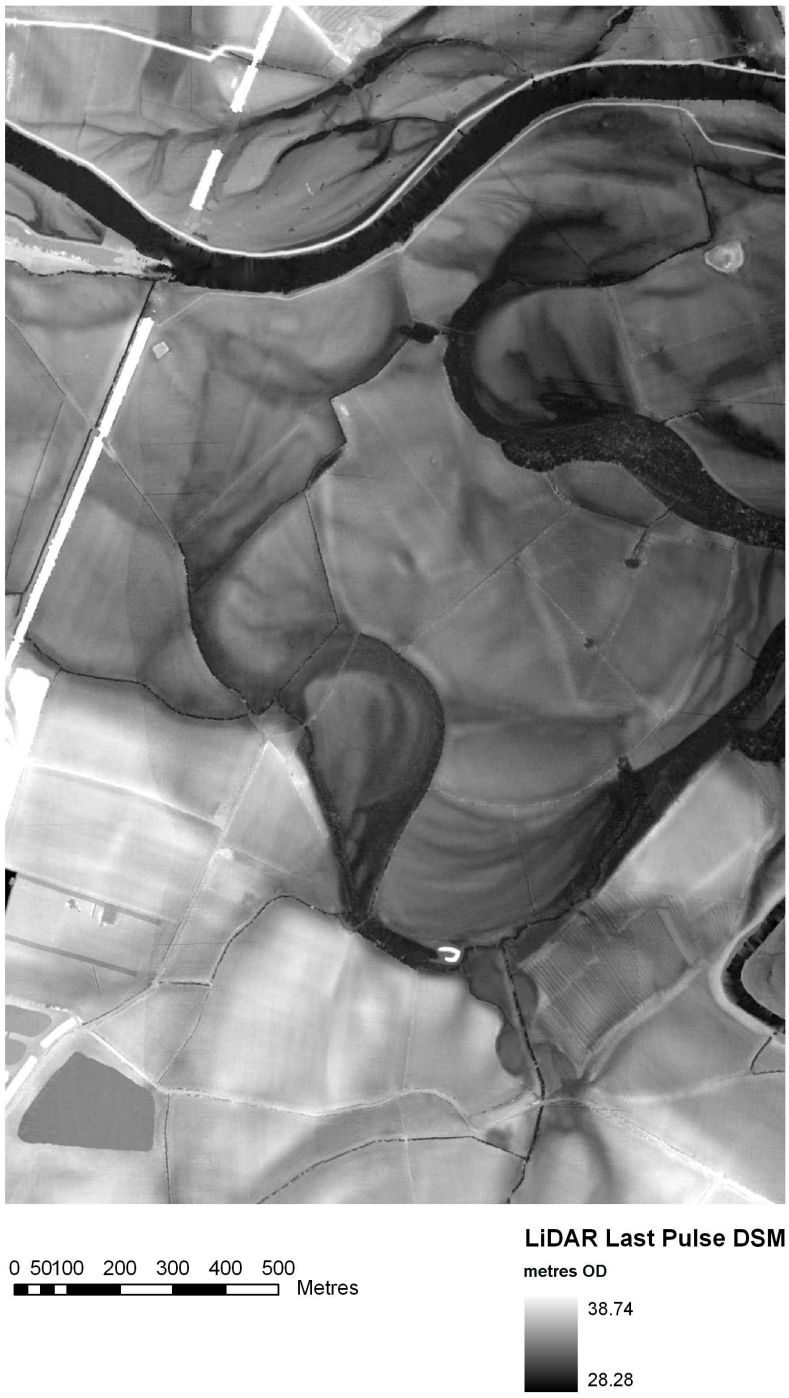


**Fig 4.12:** LiDAR last pulse ground digital surface model of the study area.

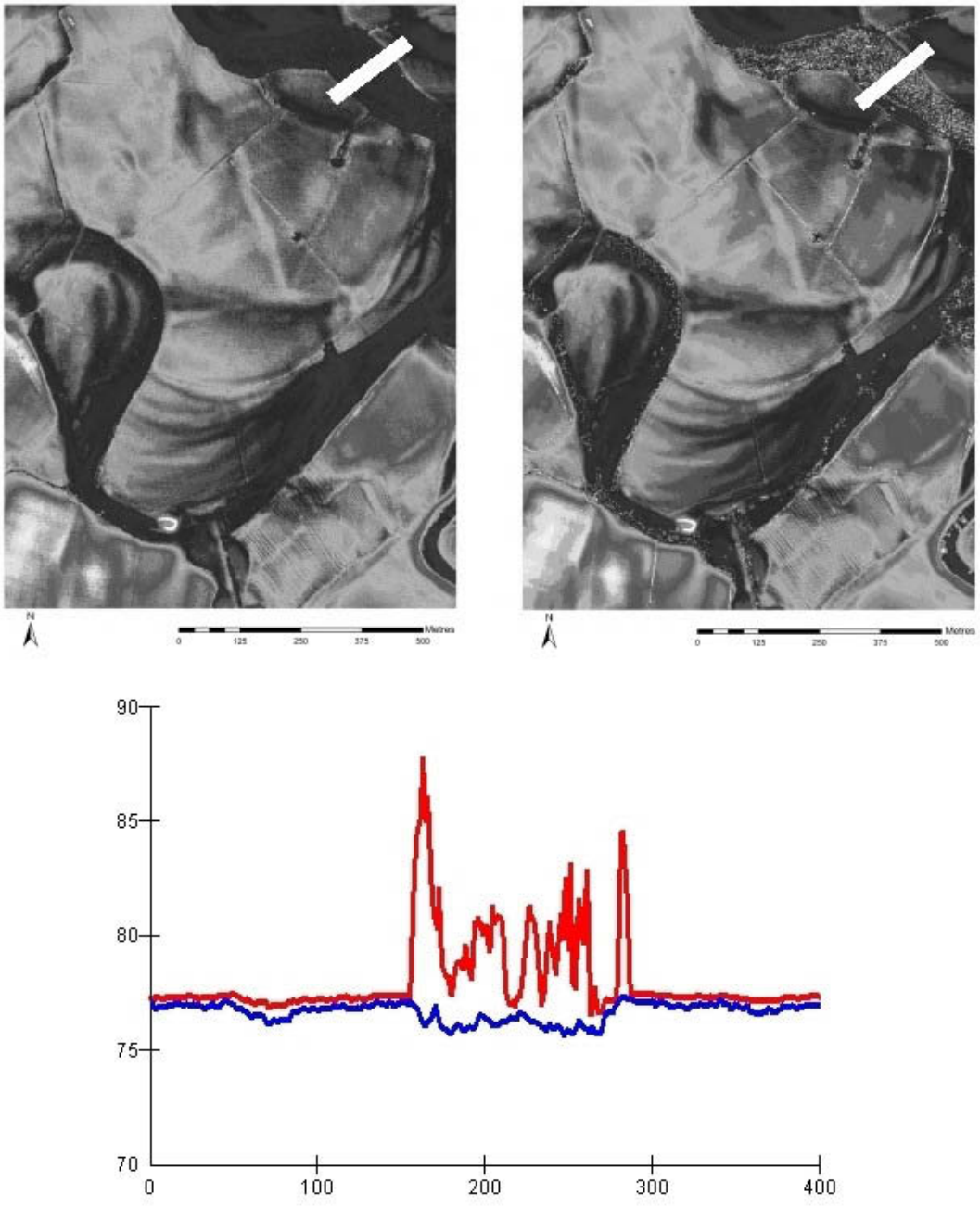


**Fig 4.13:** Last Pulse Ground (Left) and First Pulse (Right) LiDAR DSM of the study area with below profiles through the two DSM illustrating the facility of the LPG DSM to show the ground surface of palaeochannels beneath vegetation cover. Profile location shown by broad white line.


**Fig 4.14:** LiDAR laser intensity data for the study area.

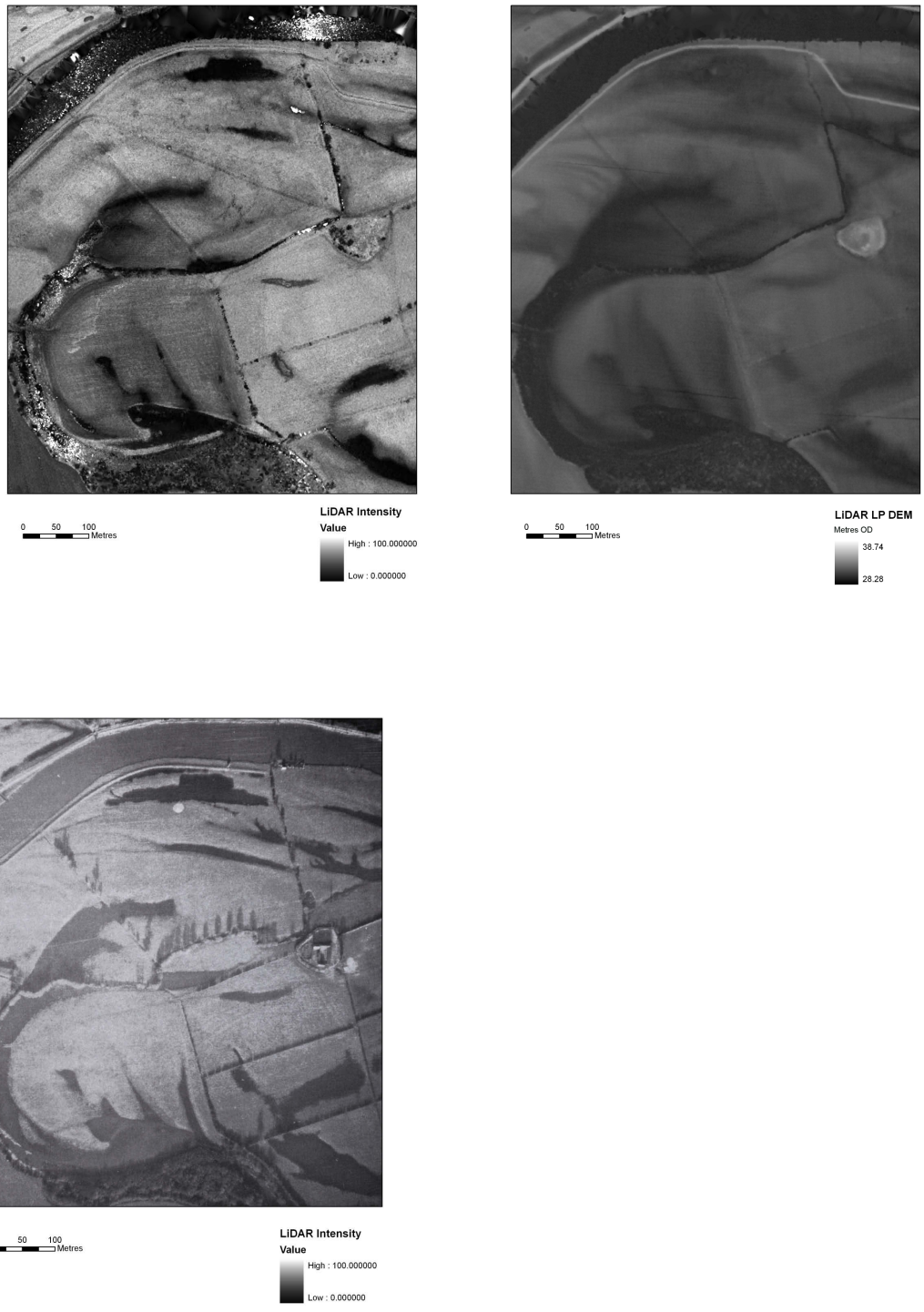


**Fig 4.15:** Comparison of (A) LiDAR laser intensity (B) LiDAR DSM and (C) air photographic evidence for palaeochannels within the floodplain and Hemington Terrace.



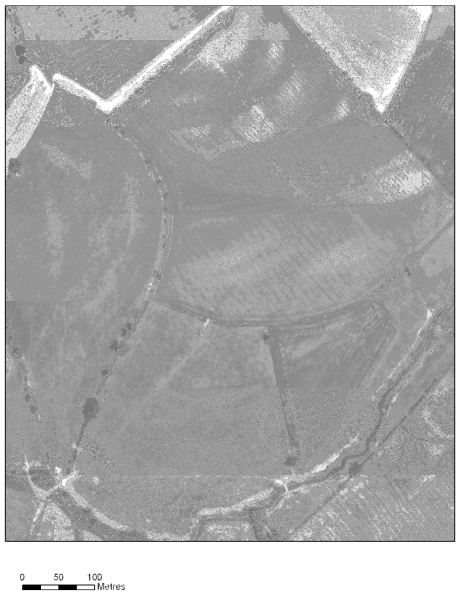


**Fig 4.16:** Comparison of (A) LiDAR laser intensity (B) LiDAR DSM and (C) air-photographic evidence for palaeochannels within the Hemington Terrace.

## 4.5 LiDAR DSM Spatial Resolution

LiDAR data was examined to determine its absolute accuracy, ability to resolve topographical features on the floodplain and terrace, and the impact of variations in spatial resolution of the elevation values on these factors. Absolute accuracy of the LiDAR elevation data was tested by comparing LiDAR LP ground elevation values, with elevation values recorded in the field using carrier phase differential GPS. Six transects across channel features were surveyed using a Leica system RD500 Real Time Kinematic Carrier Phase Differential Global Positioning System, taking elevation reading at the ground surface at approximately 0.5m intervals (Fig. 4.17: 1-6). Survey data were corrected to OSGB36 projection and orthographic elevation values conforming to Ordnance Datum using Leica Ski Pro software. The resulting elevation vales were imported into ArcGIS and their two dimensional co-ordinates used to extract elevation values from the LiDAR data at corresponding locations.

In order to test the impact of a reduction in grid resolution, the 1m LP grid was resampled to a 2m (equivalent to the resolution of the Environment Agency's standard LiDAR product) 5m and 10m grid spacing. Resampling was accomplished by extracting values from the LiDAR LP DSM at appropriate intervals. Values for the resampled grids were extracted directly from the LP DSM without averaging or otherwise calculating trends between resampled points and using these extracted values to generate a new grid at reduced resolution.

The 2m, 5m and 10m grids were compared visually to the original 1m resolution data (Figs. 4.24 – 4.28) and grid elevation and slope histograms (Figs. 4.29 and 4.30) and grid statistics for each generated (Tab. 4.2). In addition, elevation values for 1m FP and LP, 1m intensity, 2m, 5m and 10m resampled grids and 10m IFSAR elevation products were extracted for each of the six GPS survey transects used to evaluate the accuracy of the 1m DSM and a further six transects (Fig. 4.17; 6-12). Profiles generated from these extracted elevation values are shown (Fig. 4.22 – 4.23).

### *4.5.1 Absolute Accuracy of the LiDAR DSM*

Calculations of the absolute accuracy of the LiDAR DSM compared to a GPS surveyed transect proved problematic. Comparison of LiDAR and GPS derived elevation vales showed a difference in reported elevation values of between 11.68 and 12.18m (mean 11.85m). Further investigation showed that the OD values recorded by the GPS are considerably below those expected for the area surveyed. Examination of X and Y coordinate data from the GPS survey showed close coincidence of the surveyed data with map, LiDAR and air-photographic evidence. It seems likely that there is a problem with the Z co-ordinate component of the GPS survey, probably caused by the collection of insufficient differential correction data from the fixed base station (in general significantly greater data is required to produce accurate Z co-ordinated compared to X and Y). This difficulty rendered measurements of absolute accuracy of the LiDAR elevation products impossible with the data collected and analysis has therefore been limited to assessment of relative accuracy of LiDAR and GPS (i.e. how well does LiDAR record the subtleties of topography actually evident on the ground).

### *4.5.2 Relative Accuracy and Resolving Ability of the LiDAR DSM*

Visual comparison of the terrain detail captured by the 1m LiDAR LP DSM and that recorded by field survey using GPS may be made by comparing the profiles (Figs. 4.18 – 4.20). Profiles were recorded to represent a variety of terrain types including ridge and swale (P1; Fig. 4.18), palaeochannels (P2-5; Figs. 4.18 – 4.20) and terrace edge (P6; Fig. 4.20).

Ridge and Swale

The roughly parallel sinuous corrugations of ridge and swale, developed through successive southward channel migration, are clearly evident in the LiDAR intensity image on the line of profile 1 (Fig. 4.17 and 4.18). The surveyed ridges, captured by the GPS survey, are faithfully represented in the LiDAR 1m LP DSM as changes in elevation of about the correct magnitude (0.1-0.2m). High frequency variations in the LiDAR profile are likely to be the result of residual vegetation effects; in general both the detail and scale of the ridge and swale are captured by the LiDAR DSM.

Palaeochannel

Four profiles across a broad sinuous palaeochannel (up to 0.5m deep) within the Hemington terrace deposits were recorded. The channel is clearly evident on the LiDAR intensity image and forms a marked topographical feature on the ground, which is recorded by four GPS surveyed orthogonal profiles. Once again there is god agreement in both detail and scale between the LiDAR LPG DSM and the GPS profiles. All of the LiDAR profiles exhibit some high frequency noise, this particularly affects profiles 2 and 4, and is less evident on profile 5. Interestingly, the slight mid channel feature crossed by profiles 4 and 5 and evident as an area of higher intensity laser return on Fig. 4.17, is only weakly visible as a topographical feature on both the GPS and LiDAR data, but is far more clearly represented as a variation in intensity, particularly on profile 5 (Fig. 4.20).

Terrace Edge

The western edge of the Hemington terrace, where it has an erosive contact with a substantial sinuous palaeochannels of the Trent, forms a well defined topographical feature about 0.8m high. The terrace edge as surveyed in the field is faithfully captured by the LiDAR LPG DSM (P6; Fig. 4.20), although with some variation in the profile of the terrace surface evident.

## 4.6 Resolving Ability of the Resampled DSM

Resampled LiDAR DSM at 2m, 5m and 10m spatial resolution were also queried for comparison with the GPS field survey and 1m LPG DSM (Figs. 4.18 – 4.20). The effects of reduction in spatial resolution have a minimum affect at 2m resolution, although the definition of low amplitude features such as ridge and swale is reduced and the clarity with which the edges of more substantial features can be discerned is degraded. Nevertheless, for the majority of purposes the 2m spatial resolution data is suitable for the identification of features of floodplain and terrace topography, even if compromised in their accurate delineation. The general visual impression of the 2m DSM (Fig. 4.25) is good, and there appears to be little or no loss in resolution compared to the 1m data, even though only 25% of the original data remains (c 800k values as compared to 3.3million for the 1m DSM).

Casual visual inspection of the entire DSM when reduced to 5m (Figure 25) and 10m (Fig. 4.26) spatial resolution might also suggest that much of the detail captured at 1m resolution remains. This is incorrect. Examination of the profiles at 5m and 10m resolution shows that, beyond a general variation in elevation, none of the detail captures at 1m resolution survives and these low resolution DSM are completely unable to capture the form or edges of topographical features.

The effects of degradation in DSM resolution on the ability to identify and record archaeological features is shown (Figs. 4.27 and 4.28). Ridge and furrow clearly delineated at 1m resolution (Fig. 4.27), remain quite clearly defined at 2m resolution, are evident at 5m grid spacing but at 10m resolution are not recognisable. Likewise, the earthworks of the Bull Ring (Fig. 4.28) a small sub-square embanked

enclosure on the western edge of the study area, are clearly seen at 1m and 2m resolution, fading at 5m and not recognisable at 10m resolution.

Examination of DSM elevation histograms reveals something of the nature of the impact of reduction in grid resolution on the data. In each case, from 1m to 10m, the overall elevation histograms (Figs. 4.29 and 4.30) remain largely unaltered in shape as the reduction in data quantity does not drastically effect the spatial distribution of elevation values. The spatial distribution is the main contributor to these data. However, examination of frequency histograms for derived slope from each DSM does clearly highlight the main impact of reducing grid resolution: that is a decreasing ability to resolve fine variations in slope as both the range of slope values and the variation within the range decreases (Tab. 4.2) with decreasing resolution.

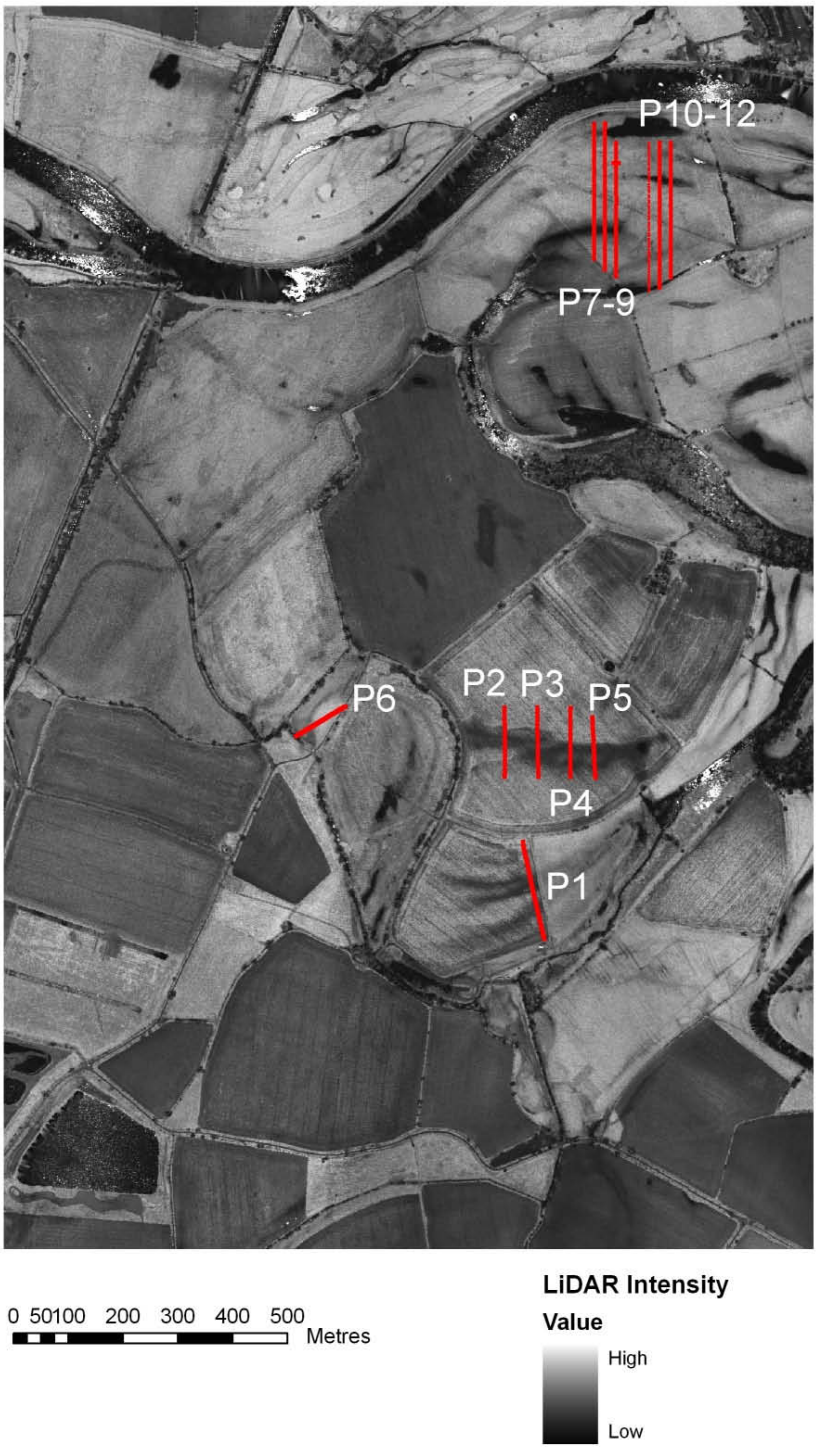


**Fig 4.17:** LiDAR laser intensity data for the study area with red lines indicating the location and extent of the 12 study transects.

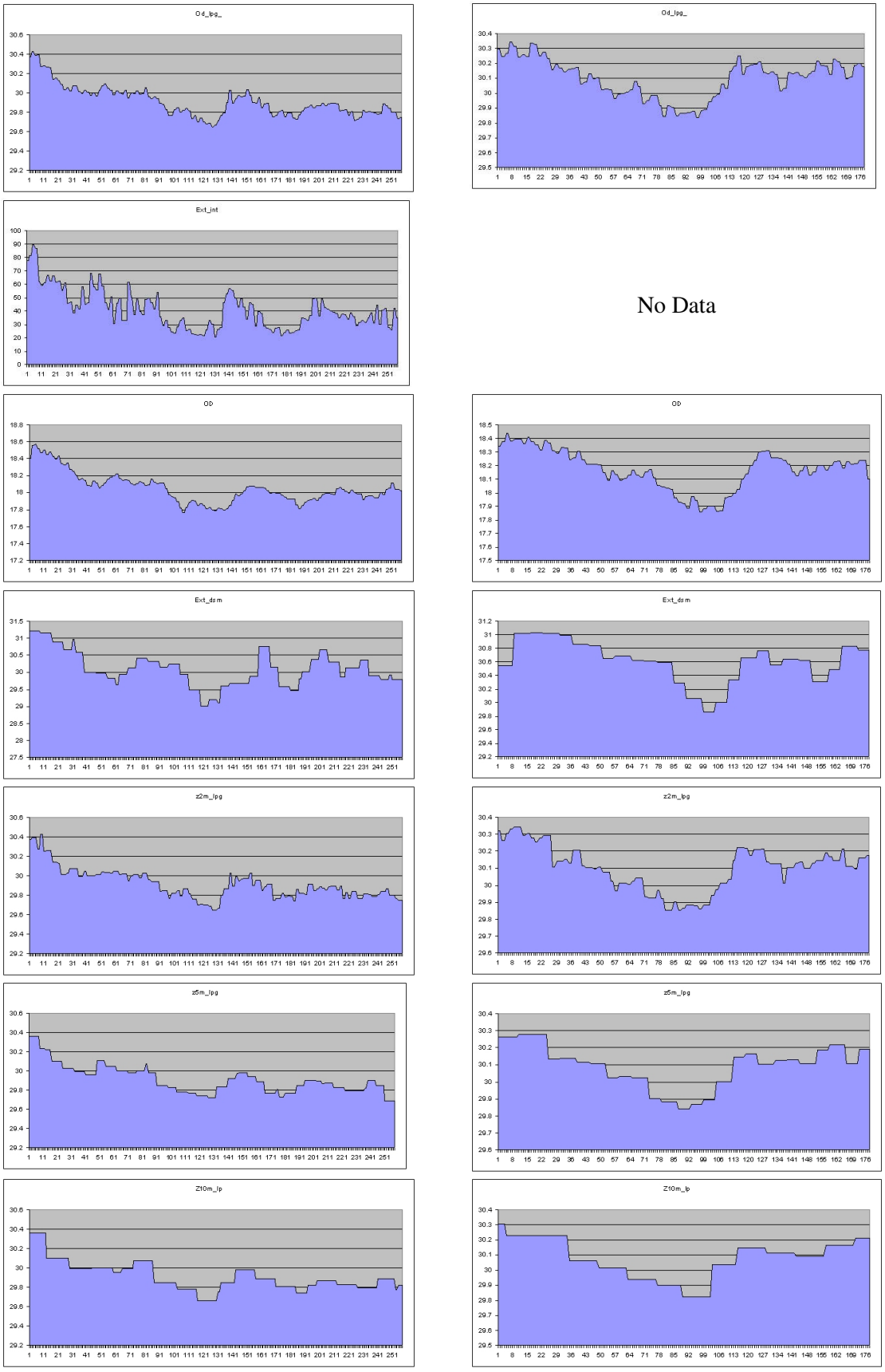


Profile 1 (T1 – ridge and swale) Profile 2 (T1 - palaeochannel)

**Fig 4.18:** Profiles 1 and 2 showing from top to bottom, RTK GPS elevation values, LiDAR LP DSM, LiDAR Intensity, IFSAR DSM, simulated 2m, 5m and 10m LiDAR DSM.

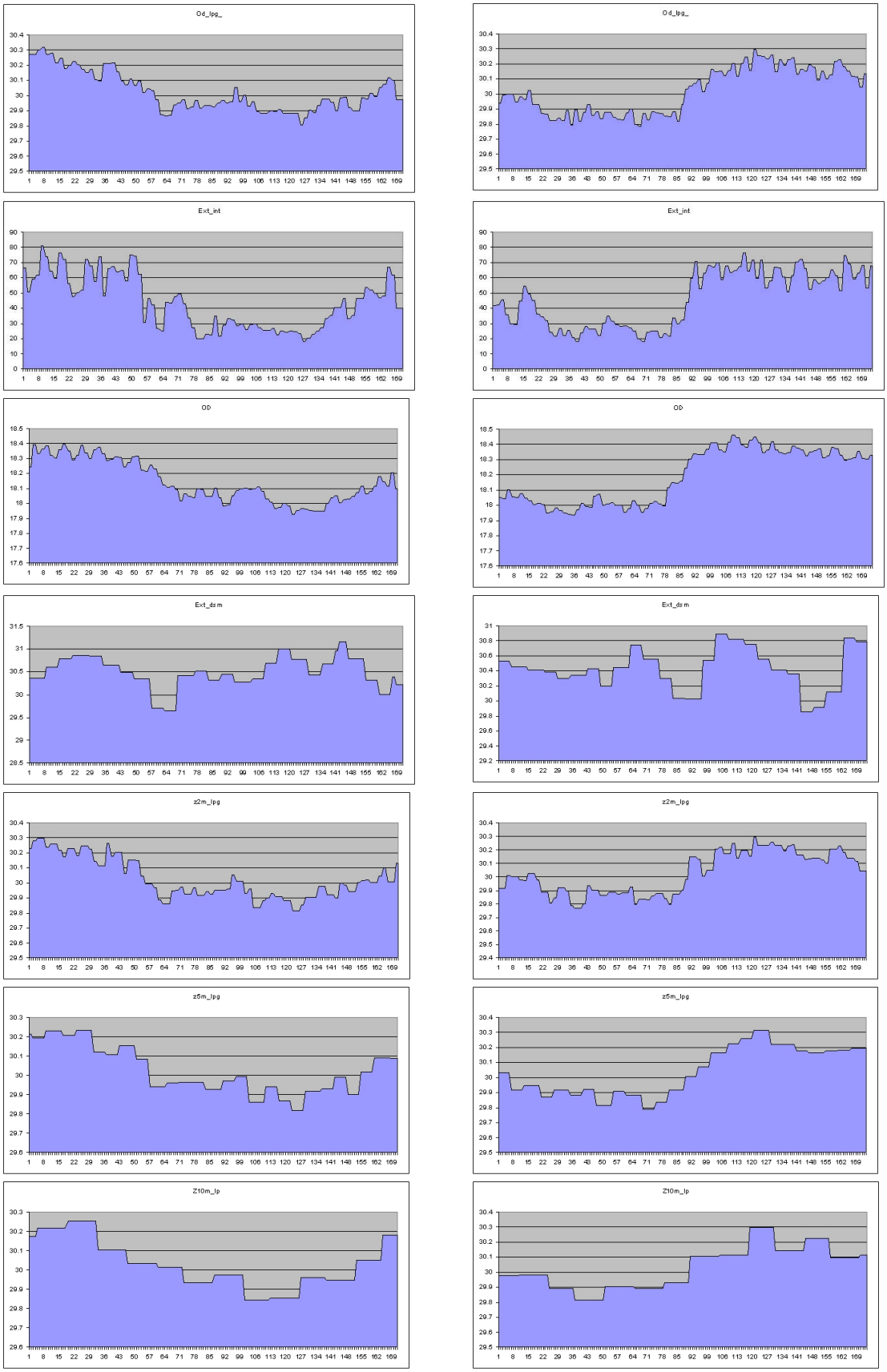


Profile 3 (T1- palaeochannel) Profile 4 (T1- palaeochannel)

**Fig 4.19:** Profiles 3 and 4 showing from top to bottom, RTK GPS elevation values, LiDAR LP DSM, LiDAR Intensity, IFSAR DSM, simulated 2m, 5m and 10m LiDAR DSM.

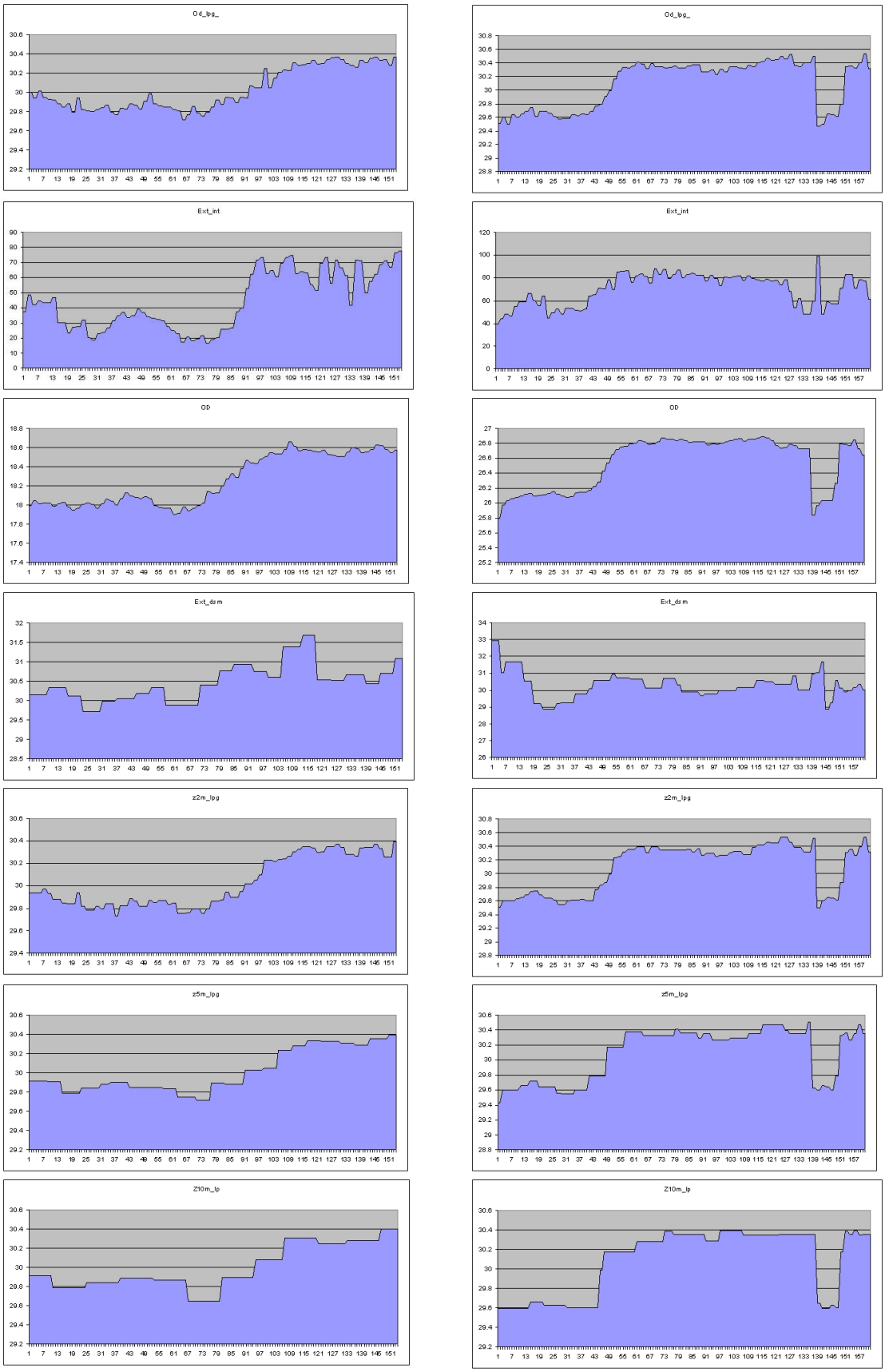


Profile 5 (T1- palaeochannel)

Profile 6 (T1 – terrace edge)

**Fig 4.20:** Profiles 5 and 6 showing from top to bottom, RTK GPS elevation values, LiDAR LP DSM, LiDAR Intensity, IFSAR DSM, simulated 2m, 5m and 10m LiDAR DSM.

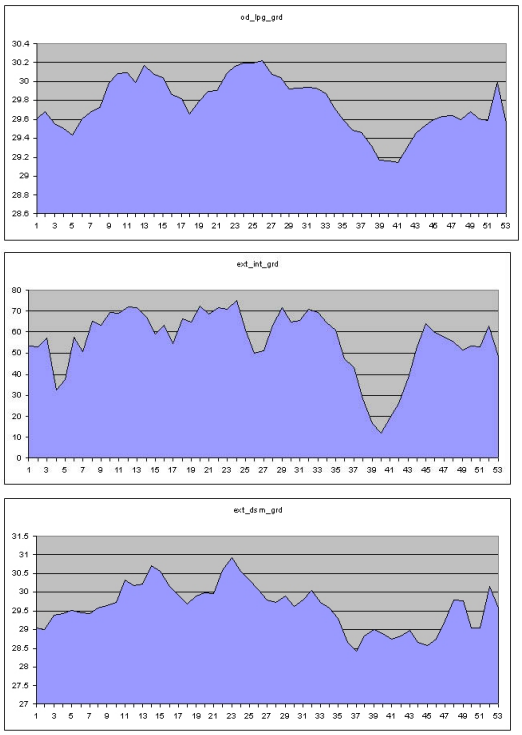


Profile 7 (MFP - palaeochannel)

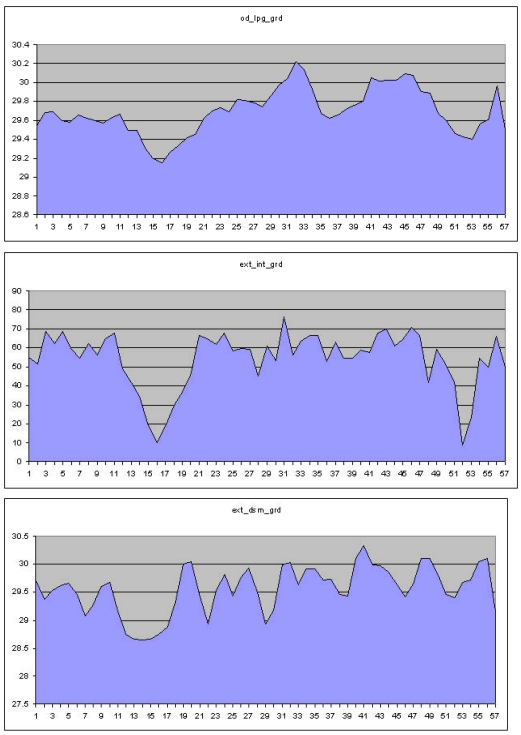


Profile 8 (MFP - palaeochannel)

**Fig 4.21:** Profiles 7 and 8 showing from top to bottom LiDAR LP DSM, LiDAR intensity and IFSAR DSM.

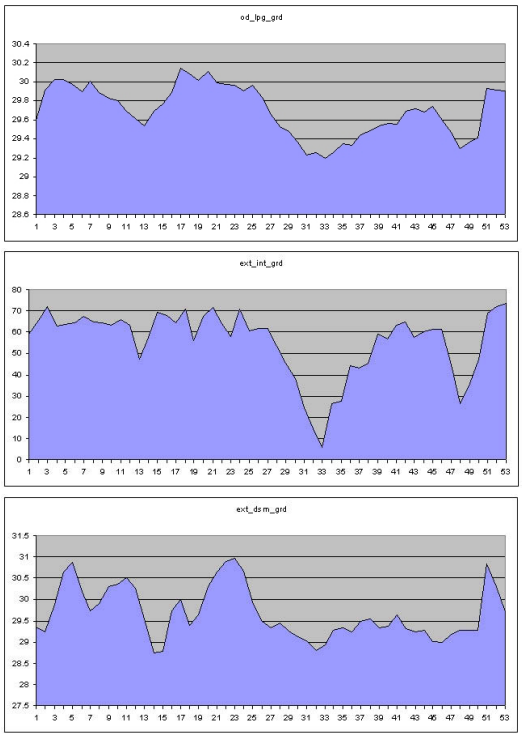


Profile 9 (MFP - palaeochannel)

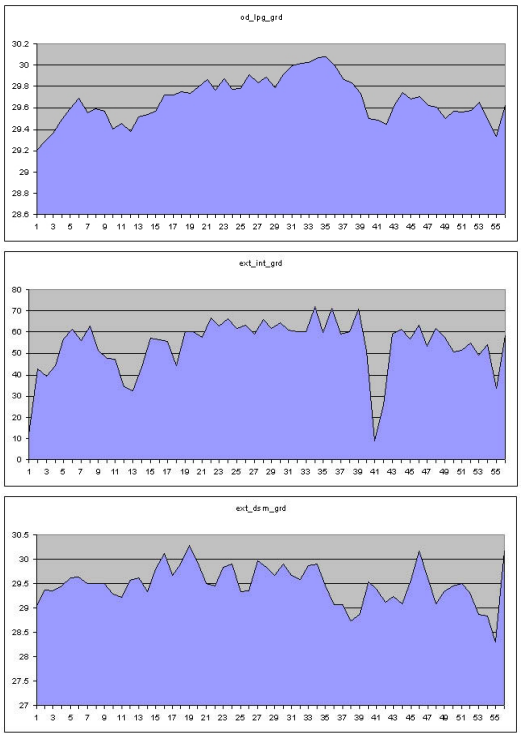


Profile 10 (MFP - palaeochannel)

**Fig 4.22:** Profiles 9 and 10 showing from top to bottom LiDAR LP DSM, LiDAR intensity and IFSAR DSM.

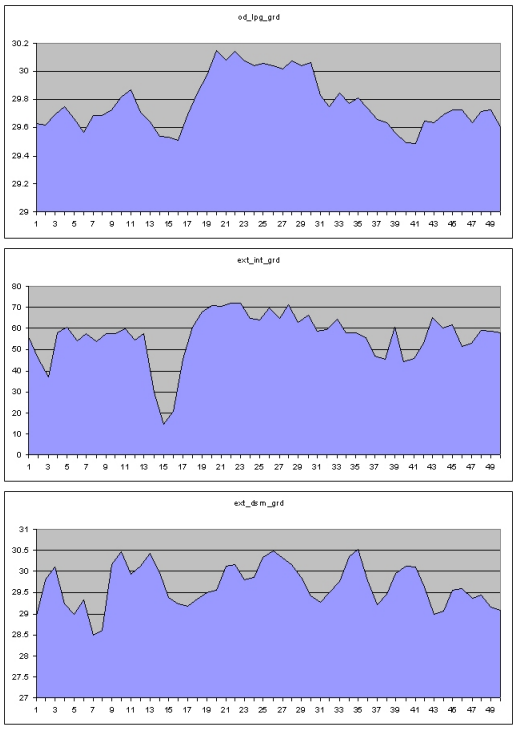


Profile 11 (MFP - palaeochannel)

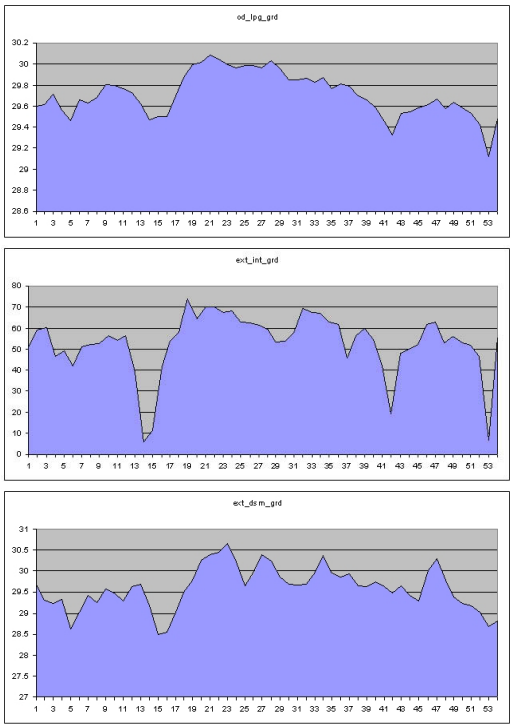


Profile 12 (MFP - palaeochannel)

**Fig 4.23:** Profiles 11 and 12 showing from top to bottom LiDAR LP DSM, LiDAR intensity and IFSAR DSM.

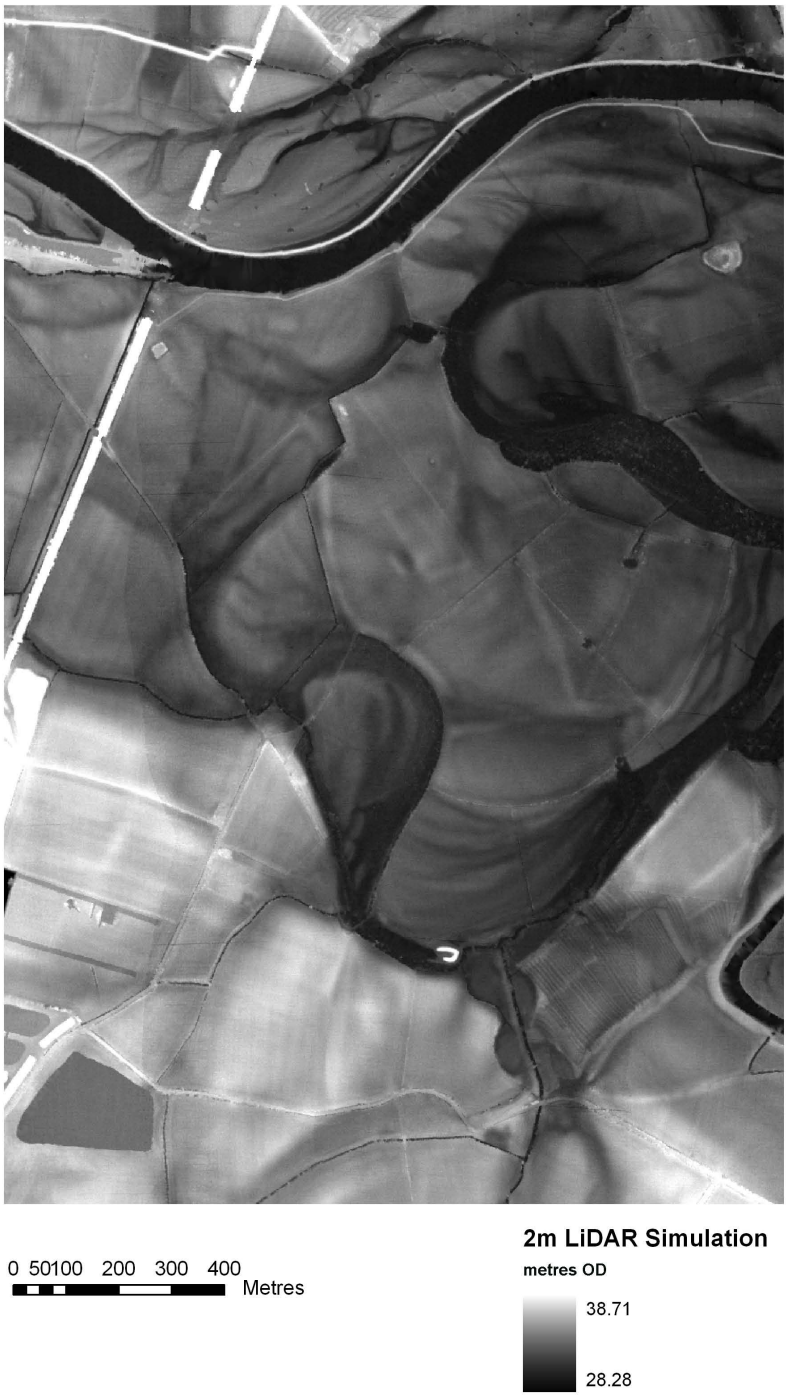


**Fig 4.24:** Simulated 2m LiDAR Last pulse ground digital surface model.


**Fig 4.25:** Simulated 5m LiDAR Last pulse ground digital surface model.